

Coherent processes in electromagnetically induced absorption: a steady and transient study

This content has been downloaded from IOPscience. Please scroll down to see the full text.

2011 New J. Phys. 13 033010

(<http://iopscience.iop.org/1367-2630/13/3/033010>)

View [the table of contents for this issue](#), or go to the [journal homepage](#) for more

Download details:

IP Address: 147.91.1.42

This content was downloaded on 04/04/2016 at 13:58

Please note that [terms and conditions apply](#).

Coherent processes in electromagnetically induced absorption: a steady and transient study

J Dimitrijević¹, D Arsenović and B M Jelenković

Institute of Physics, University of Belgrade, Pregrevica 118,
10080 Belgrade, Serbia

E-mail: jelena.dimitrijevic@ipb.ac.rs

New Journal of Physics **13** (2011) 033010 (15pp)

Received 23 September 2010

Published 8 March 2011

Online at <http://www.njp.org/>

doi:10.1088/1367-2630/13/3/033010

Abstract. A perturbation method was used to solve optical Bloch equations (OBEs) for the transition $F_g = 1 \rightarrow F_e = 2$, in order to describe the role of ground-level Zeeman coherences in the formation of electromagnetically induced absorption (EIA). A narrow Lorentzian peak, centered at zero value of the scanning magnetic field, appears in the analytical expression of the second-order correction of a density-matrix element for ground-level Zeeman coherences, $(\rho_{g-1,g+1})_{x_2}$. Through analytical expressions for lower-order corrections of density-matrix elements, we were able to establish clear relations between the narrow Lorentzian in $(\rho_{g-1,g+1})_{x_2}$ and higher-order corrections of optical coherences, i.e. EIA. We see from analytical expressions that these two resonances have opposite signs and that EIA becomes electromagnetically induced transparency (EIT) in the limit of low efficiency of spontaneous transfer of coherences from excited-level to ground-level Zeeman sublevels. The transient behavior of EIA follows the time evolution of $(\rho_{g-1,g+1})_{x_2}$. After the coupling laser is turned on, both the Lorentzian peak in $(\rho_{g-1,g+1})_{x_2}$ and EIA reach steady state via over-damped oscillations.

¹ Author to whom any correspondence should be addressed.

Contents

1. Introduction	2
2. Optical Bloch equations and the perturbation method for the $F_g = 1 \rightarrow F_e = 2$ transition	3
3. Results and discussion	5
3.1. Steady-state electromagnetically induced absorption	5
3.2. Transient evolution of electromagnetically induced absorption	8
4. Conclusion	12
Acknowledgments	12
Appendix A. Optical Bloch equations	13
Appendix B. Derivation of equation (5)	13
References	14

1. Introduction

Coherent phenomena such as coherent population trapping (CPT) [1]–[3] and the cancellation of light absorption, as manifested by electromagnetically induced transmission (EIT) [4], continue to attract great attention. But under certain laser–atom interaction schemes (multi-V-schemes, for example), coherence interaction can lead to increased absorption, giving rise to electromagnetically induced absorption (EIA) [5]. EIA is observed under the condition that lasers couple two degenerate atomic levels and that the angular moment of the excited state is higher than that of the ground state, $F_g = F \rightarrow F_e = F + 1$ [6]. More recently, EIA was observed [7, 8] in open systems and in systems for which $F_e = F_g - 1$ and $F_g = F_e$ stand, and models were developed to interpret this ‘anomalous’ EIA [9].

For a closed transition interacting with a single-frequency field, it was shown [10] that EIA is due to the redistribution of atomic population among ground-state Zeeman sublevels—by optical pumping of atomic population in the ground states which are maximally coupled to the excited state. For a pump–probe excitation of a degenerate two-level system, EIA may also occur due to the transfer of coherence through spontaneous emission from the excited state [11, 12]. Using an N -configuration atom, Taichenachev *et al* [12] have shown that the sign of the absorption resonance can change, depending on the rate of coherence transfer, and that EIA can turn into enhanced transmission in the case of zero or even a low rate of coherence transfer. EIA in an N -type interaction scheme has also been investigated for various pump and probe intensities with and without transfer of coherence and Doppler broadening in [13], both analytically and numerically. The results were compared with the results obtained for realistic atomic systems.

It was also shown that the transfer of coherence can give rise to EIA when the pump and probe photons have different polarizations, and when ground-state population trapping does not occur [14]. The authors of [14] have shown that EIA, which is due to the transfer of population, can develop in an open system, with the same pump and probe polarizations. For the latter mechanism to occur, collisional transfer of population from the ground state to a reservoir (a nearby hyperfine level that does not interact with the pump) should be greater than that from the excited state. The same group recently analyzed [15] the relation between ground-state

coherences and EIA in the pump–probe configuration. They have shown numerically that the spectroscopic signal depends on ground- and excited-state populations and Zeeman coherences. The role played by transfer of coherence from the excited to the ground hyperfine state was also analyzed. Our previous work on phenomena of enhanced absorption includes the investigation of EIA amplitudes and linewidths as a function of different parameters, such as laser intensity, polarization and transverse magnetic fields [16]–[18].

Although the temporal evolution of CPT has been thoroughly studied [19]–[21], the transient properties of EIA have only been sparsely investigated. The transmission of a fixed frequency laser beam for sudden turn on and off of a static magnetic field was studied in [22] and the temporal evolution of EIA in the pump–probe spectroscopy of a degenerate two-level atomic transition was studied in [23].

In this paper, we use analytical expressions for density-matrix elements, obtained by applying the perturbation method to the closed multilevel $F_g = 1 \rightarrow F_e = 2$ transition, in the Hanle configuration, to study the development of EIA. The analytical expressions of low-order corrections of density-matrix elements provide valuable information on the mechanisms that are important for induction of EIA which cannot be deduced from numerical solutions of the optical Bloch equations (OBEs) for the same multilevel atomic system. We particularly investigate the importance of a narrow Lorentzian peak, found in the steady-state analytical expression of ground-state coherence $(\rho_{g_{-1},g_{+1}})_{x_2}$ as a function of external magnetic field, on the overall behavior of EIA. The effectiveness of coherence transfer to the excited-state Zeeman sublevels, and subsequent spontaneous coherence transfer from the excited state, was for the first time explicitly presented. The relation between ground-level Zeeman coherences and EIA was also investigated in the transient regime for external magnetic fields smaller and larger than the magnetic field corresponding to the linewidth of the narrow Lorentzian in $(\rho_{g_{-1},g_{+1}})_{x_2}$.

2. Optical Bloch equations and the perturbation method for the $F_g = 1 \rightarrow F_e = 2$ transition

Density matrix $\hat{\rho}$ is calculated from OBEs:

$$\frac{d\hat{\rho}(t)}{dt} = -\frac{i}{\hbar}[\hat{H}_0, \hat{\rho}(t)] - \frac{i}{\hbar}[\hat{H}_I, \hat{\rho}(t)] - \hat{S}\hat{E}(b)\hat{\rho}(t) - \gamma\hat{\rho}(t) + \gamma\hat{\rho}_0, \quad (1)$$

for the $F_g = 1 \rightarrow F_e = 2$ atomic transition (see figure 1). OBEs in explicit form are given in appendix A. Diagonal elements of $\hat{\rho}$, ρ_{g_i,g_i} and ρ_{e_i,e_i} are populations, while ρ_{g_i,g_j} and ρ_{e_i,e_j} are Zeeman coherences. Indices g and e stand for the ground and excited levels (see figure 1). Elements ρ_{g_i,e_j} and ρ_{e_i,g_j} are optical coherences, and in the rotating wave approximation the usual substitution $\rho_{e_i,g_j} = \tilde{\rho}_{e_i,g_j}(e)^{-i\omega t}$ is introduced, where ω is the laser frequency. \hat{H}_I is the interaction Hamiltonian, characterized by the Rabi frequency Ω , which is proportional to the magnitude of the laser electric field \mathbf{E} , and by the ellipticity ϵ . Linearly polarized laser light propagates parallel to the direction of static magnetic field \mathbf{B}_s . The quantization axis is chosen parallel to the magnetic field. The interaction with the magnetic field B_s is given by the Hamiltonian part \hat{H}_0 . The energies describing the Zeeman splitting of the ground and excited levels with magnetic quantum numbers $m_{g(e)}$, $E_{g(e)} = \omega_{g(e)}\hbar$, due to applied magnetic field B_s , were calculated by using $E_{g(e)} = \mu_B l_{F_{g(e)}} m_{g(e)} B_s$. Here μ_B is the Bohr magneton and $l_{F_{g,e}}$ is the Lande gyromagnetic factor for two hyperfine levels. $\hat{S}\hat{E}(b)$ is the abbreviated spontaneous emission operator whose rate is Γ . The parameter $0 \leq b \leq 1$ describes the efficiency of the

$$F_e = 2 \quad \frac{|e_{-2}\rangle}{\quad} \quad \frac{|e_{-1}\rangle}{\quad} \quad \frac{|e_0\rangle}{\quad} \quad \frac{|e_{+1}\rangle}{\quad} \quad \frac{|e_{+2}\rangle}{\quad}$$

$$F_g = 1 \quad \frac{|g_{-1}\rangle}{\quad} \quad \frac{|g_0\rangle}{\quad} \quad \frac{|g_{+1}\rangle}{\quad}$$

Figure 1. $F_g = 1$ and $F_e = 2$ hyperfine levels with notation of magnetic sublevels.

transfer of coherences from excited to ground sublevels due to spontaneous emission; $b = 0$ means no transfer, while $b = 1$ means a complete spontaneous transfer of coherence. The term $\gamma \hat{\rho}$ describes the relaxation of all density-matrix elements due to the finite time for an atom to cross the laser beam. The continuous flux of atoms to the laser beam, with equal population of three ground Zeeman sublevels, is described by $\gamma \hat{\rho}_0$. The role of laser detuning (and Doppler broadening) is not discussed.

Macroscopic polarization of atomic media, calculated from

$$\mathbf{P} = N \langle e\mathbf{r} \rangle = Ne \text{Tr}(\hat{\rho} \hat{\mathbf{r}}) \quad (2)$$

gives complex susceptibility χ expressed as a sum of optical coherences. The imaginary part of χ represents loss per unit wavelength, i.e. the absorption coefficient [24]. The constant N in equation (2) stands for atomic concentration, and is irrelevant in this study. By EIA in the following text, we mean the absorption coefficient calculated by using equation (2).

We use the perturbation method for both the steady-state (by taking the left-hand side of equation (1) equal to 0) and time-dependent solution of equation (1). We start from time-dependent OBEs in matrix form, $\dot{x}(t) = Ax(t) - y$, where x represents the column of density-matrix elements sorted as $\{\rho_{g_{-1},g_{-1}}, \rho_{g_{-1},g_0} \dots \rho_{e_{+2},e_{+2}}\}$; A is the system's matrix and y is the non-homogeneous part. We separate A into the unperturbed and perturbed parts, $A = A_0 + A_{\text{pert}}$. Since the interaction of an atom with the laser light's field is considered a perturbation [25, 26], we have the following: (a) all terms with Rabi frequencies belong to the matrix A_{pert} and (b) the elements of A_{pert} are much smaller than those of A_0 ($\Omega \ll \Gamma$). Solutions of the time-dependent OBEs obtained by the perturbation method are

$$\begin{aligned} \dot{x}_0(t) &= A_0 x_0(t) - y, \\ \dot{x}_{n+1}(t) &= A_0 x_{n+1}(t) + A_{\text{pert}} x_n(t). \end{aligned} \quad (3)$$

By taking the left-hand sides equal to 0 in previous equations, the solutions of the steady-state OBEs are

$$\begin{aligned} x_0 &= -A_0^{-1} y, \\ x_{n+1} &= -A_0^{-1} A_{\text{pert}} x_n. \end{aligned} \quad (4)$$

For any density-matrix element, the solution of the method has an unperturbed part x_0 and a series of successive corrections of the density matrix x_n , where n is the iteration number. The solutions of the perturbation method, x_n from equations (3) and (4), are such that each density matrix can have only even or only odd non-zero corrections. In the case of small perturbations, Ω smaller than $\simeq 0.03\Gamma$, each density-matrix element is dominantly determined by its first non-zero correction, and the sum of the non-perturbed part and corrections converges quickly

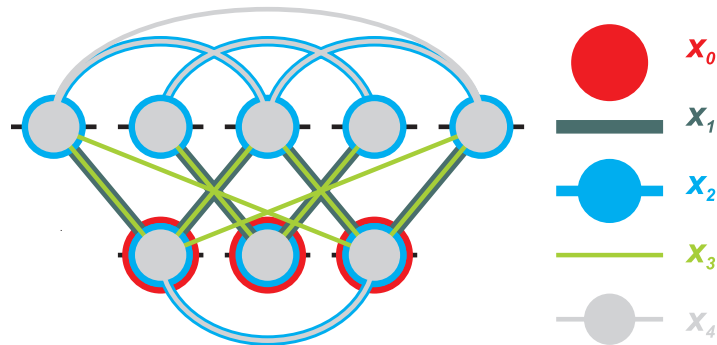


Figure 2. Schematic diagram showing which density-matrix elements are corrected by solutions of the unperturbed part x_0 and successive corrections from x_1 to x_4 . The scheme is for the transition $F_g = 1 \rightarrow F_e = 2$. Lines indicate coherences, whereas circles are populations. For notation of magnetic sublevels, see figure 1.

to the exact solutions of OBEs. By exact, we mean the numerical solution of a system of linear (differential) equations given in equation (1) for the full atomic system (given in figure 1).

The order of appearance of non-zero corrections of density-matrix elements, either even or odd, is schematically (by the column of symbols in the right of the figure) shown in figure 2. The solution of the unperturbed part x_0 is the redistribution of the ground-state populations, $1/3$ for each ground-state sublevel, the same as the initial condition for time-dependent OBEs. The first correction x_1 is non-zero only for optical coherences, for which the selection rule between magnetic sublevels $\Delta m_{g,e} = \pm 1$ stands. The second correction applies for all populations and also for Zeeman coherences of the sublevels such that $\Delta m_{g,g} = \pm 2$ or $\Delta m_{e,e} = \pm 2$. The third and all higher-order odd corrections correct all optical coherences, while fourth and all higher-order even corrections correct all populations and all Zeeman coherences of the transition $F_g = 1 \rightarrow F_e = 2$. By all we mean the coherences that are coupled by linearly polarized light, therefore being non-zero by the exact and the perturbative solution of the OBEs. As seen from figure 2, each odd correction is a new contribution to optical coherence, while even corrections bring new contributions to populations and Zeeman coherences via additional level couplings.

3. Results and discussion

3.1. Steady-state electromagnetically induced absorption

In the perturbation method, EIA appears after including the higher-order ($n \geq 3$) corrections, the odd corrections of absorption coefficient or the even corrections of excited-state populations (observable as fluorescence). The perturbation method also shows that already the second correction of ground-level Zeeman coherences, $\rho_{g-1,g+1}$ and $\rho_{g+1,g-1}$ as a function of magnetic field B_s , has a narrow resonance, a complex Lorentzian (CL). In the following, we show that the Lorentzian-like behavior of $(\rho_{g-1,g+1})_{x_2}$ is responsible for the appearance of EIA in higher-order corrections.

The analytical expression for $(\rho_{g_{-1},g_{+1}})_{x_2}$ is the sum of products of two and three CLs:

$$(\rho_{g_{-1},g_{+1}})_{x_2} = \frac{(\epsilon^2 - 1)\Omega^2}{45} \frac{1}{(\gamma - i\frac{2l_{F_g}\mu_B}{\hbar}B_s)} \left\{ \frac{2}{(2\gamma + \Gamma - i\frac{2l_{F_g}\mu_B}{\hbar}B_s)} + \frac{b\Gamma}{(\gamma + \Gamma - i\frac{2l_{F_g}\mu_B}{\hbar}B_s)} \right. \\ \left. \times \left[\frac{2}{(2\gamma + \Gamma - i\frac{2(2l_{F_c} - l_{F_g})\mu_B}{\hbar}B_s)} + \frac{3}{(2\gamma + \Gamma - i\frac{2l_{F_c}\mu_B}{\hbar}B_s)} + \frac{2}{(2\gamma + \Gamma - i\frac{2l_{F_g}\mu_B}{\hbar}B_s)} \right] \right\}, \quad (5)$$

while $(\rho_{g_{+1},g_{-1}})_{x_2}$ is the complex conjugate. The derivation of equation (5) is explained in appendix B. The terms within curly brackets in equation (5) contain wide CLs since $\Gamma \gg \gamma$. For the values of magnetic field within EIA, the sum of products inside the curly brackets is nearly constant and wide CLs can be approximated with $\frac{1}{\Gamma}$. Then $(\rho_{g_{-1},g_{+1}})_{x_2}$, as a function of magnetic field, can be written as

$$nCL(B_s) = \frac{(\epsilon^2 - 1)\Omega^2(-2 + 7b)}{45\Gamma} \frac{1}{\gamma \pm i\frac{2l_{F_g}\mu_B}{\hbar}B_s} \\ = \frac{(\epsilon^2 - 1)\Omega^2(-2 + 7b)}{45\Gamma} \frac{\gamma \mp 2il_{F_g}B_s\mu_B}{\gamma^2 + \frac{4l_{F_g}^2\mu_B^2}{\hbar^2}B_s^2}, \quad (6)$$

i.e. a single narrow complex Lorentzian (nCL). Here, lower sign is for $\rho_{g_{-1},g_{+1}}$ and upper is for $\rho_{g_{+1},g_{-1}}$. The full-width at half-maximum (FWHM) of $nCL(B_s)$ is equal to $\frac{\gamma\hbar}{l_{F_g}\mu_B}$ and its amplitude is $\frac{(\epsilon^2-1)\Omega^2(-2+7b)}{45\Gamma\gamma}$. Since only the real part affects absorption, we consider only the real part of $nCL(B_s)$ for amplitudes and FWHMs.

The nCL (we will omit dependence on B_s in the following text) appearing in $(\rho_{g_{+1},g_{-1}})_{x_2}$ is transferred to the other coherences and to the populations by the iterative procedure given in section 2 and schematically presented in figure 2. Note that this transfer to the next successive correction is only to the density-matrix elements which, according to equation (4), depend on $(\rho_{g_{-1},g_{+1}})_{x_2}$.

In figure 3 we have plotted the corrections and the sums of corrections for the absorption coefficient (EIA) as a function of external magnetic field. For comparison, the absorption coefficient from the exact solution of the OBEs is also presented. Figure 3 shows that the narrow Lorentzian first appears in the third correction of the absorption coefficient. The observed EIA is due to nCL of $(\rho_{g_{-1},g_{+1}})_{x_2}$ transferred to optical coherences, and superimposed on a broader pedestal which originated from the first-order correction of the absorption coefficient. As seen in figure 3, the narrow peak developed in the third correction is numerically almost equal to the EIA obtained from the exact solution of the OBEs.

The results presented in figure 4 compare the properties of the real part of $(\rho_{g_{-1},g_{+1}})_{x_2}$ (equation (5)) and of the exact solution for EIA. The FWHMs and amplitudes of two resonances were obtained from fits to the sum of wide and narrow Lorentzians. We show the dependences of the FWHMs and amplitudes on Rabi frequency Ω (panels (a) and (b)), relaxation rate γ (panels (c) and (d)) and the efficiency of spontaneous transfer of coherences b (panels (e) and (f)). When not variable, parameters in the calculations have values such as $\Gamma = 2\pi 6$ MHz,

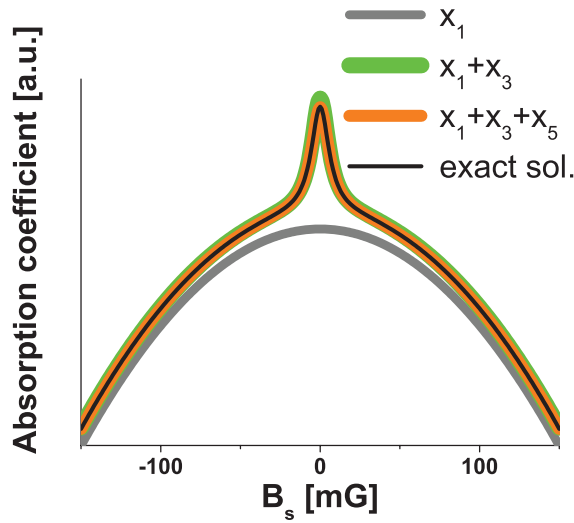


Figure 3. EIA as a function of external magnetic field. The results obtained by using the perturbation method (first non-zero correction and sums of successive corrections) and the exact solutions of the OBEs are presented. The results are for the linearly polarized light, $\Gamma = 2\pi 6$ MHz, $\Omega = 0.015\Gamma$ and $\gamma = 0.003\Gamma$.

$\Omega = 0.015\Gamma$, $\gamma = 0.003\Gamma$, $\epsilon = 0$ and $b = 1$. Note that EIA's sign differs from the sign of the real part of $(\rho_{g-1,g+1})_{x_2}$. Flat dependence of FWHM on Ω in figure 4(a) is because $(\rho_{g-1,g+1})_{x_2}$ is invariant with respect to Ω^2 , whereas the dependence of EIA's amplitude on Ω is proportional to Ω^2 (see equation (6)). The dependence on the relaxation rate γ , given in (c) and (d), shows nearly identical behavior of both $(\rho_{g-1,g+1})_{x_2}$ and the exact EIA. The dependence of amplitude can be approximated as $\sim \frac{1}{\gamma}$ and of FWHM as $\sim \gamma$ (see equation (6)). The increase of relaxation rate leads to the loss of ground-level coherences and to the consequential decrease of EIA amplitude.

As presented in equation (6), the sign of nCL is determined by parameter b . We see in figure 4(f) that the change of b from 1 to zero causes the change of sign of the resonance from EIA to EIT. For $b = \frac{2}{7}$, both $(\rho_{g-1,g+1})_{x_2}$ and the exact solution for EIA change signs. Note that this EIT is not due to CPT, since the transition $F_g = 1 \rightarrow F_e = 2$ does not have 'dark states' (noninteracting states given by $\hat{H}_1|DS\rangle = 0$) [2, 27, 28] among the ground-state sublevels. This is analogous to the result obtained in [12] which uses the N -atomic scheme. In [12], the role of the ground-state Zeeman coherence, transfer to the excited-state coherence was not discussed. In [13], it was shown that the transfer of coherences can affect the whole spectrum, not only the EIA peak. The spontaneous transfer of Zeeman coherences from the excited to ground levels influences, as shown in [11], the nonlinear resonances in probe-field spectroscopy. The transfer of coherences can be neglected [29] if excited states are far apart in energy.

Although approximative, the perturbative method gives important nontrivial results. The EIA amplitudes and widths can be very well approximated from a simple analytical expression for $(\rho_{g-1,g+1})_{x_2}$. Also, from the analytical expression for the third correction of the absorption coefficient (not shown here), we can see that the term for the narrow Lorentzian in the EIA is the same (with opposite sign) Lorentzian present in $(\rho_{g-1,g+1})_{x_2}$.

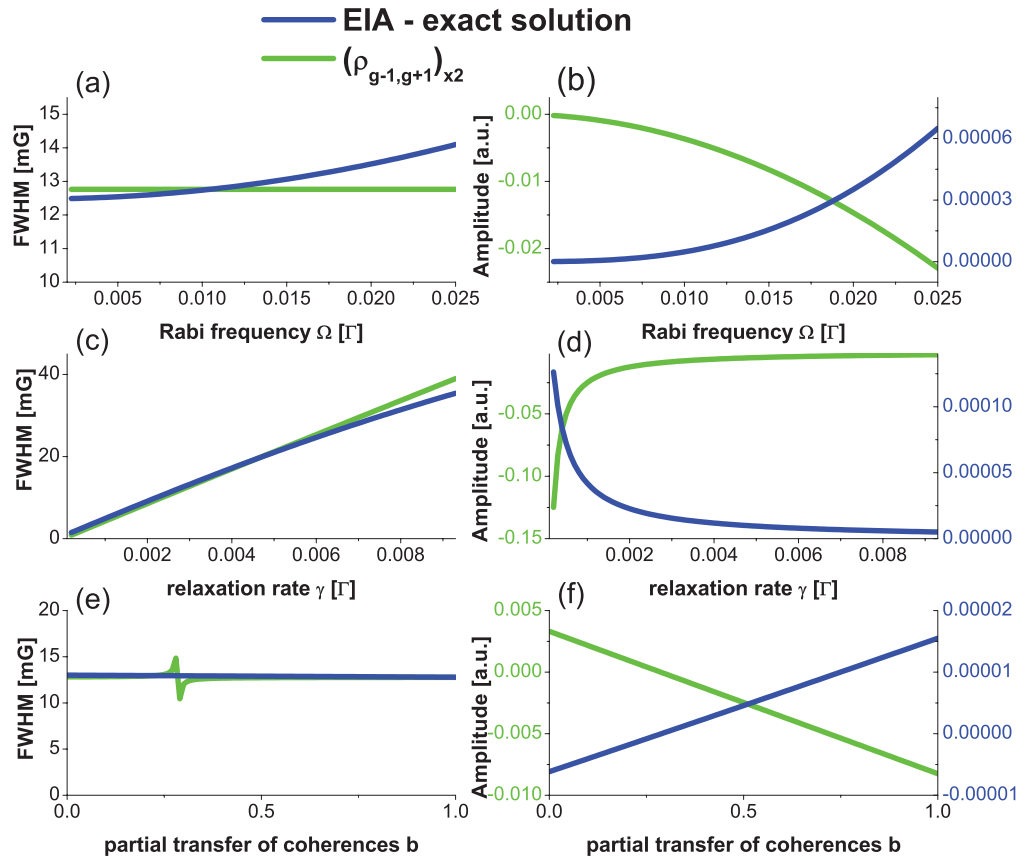


Figure 4. Comparison of the FWHM (left column) and the amplitude (right column) obtained from profiles of the EIA, i.e. absorption coefficient (blue curves) and the real part of $(\rho_{g-1,g+1})_{x_2}$ (green curves). Various parameters were varied—Rabi frequency, relaxation rate and efficiency of spontaneous transfer of coherences. Note that, in the right column, there are different scales for amplitudes indicated with different colors (blue and green). In panel (e), there are few evasions that are due to the error of fitting.

3.2. Transient evolution of electromagnetically induced absorption

In figure 5, we present the exact solution of the evolution of the EIA as a function of magnetic field and time after sudden application of the laser field. The transient behavior of EIA is different from the behavior of the rest of the wide pedestal of the absorption coefficient: while the evolution of EIA shows no oscillations, the evolution of other parts of the absorption coefficient shows small oscillations. The model for the probe absorption in the pump–probe configuration based on the N -atomic scheme [23] shows a central peak with oscillating wings, such as the Hanle EIA in figure 5.

The perturbation method can explain the observed transient behavior of the absorption coefficient through simple analytical expressions. By using equation (3) first by differentiating $\dot{x}_{n+1}(t)$ and then substituting $\dot{x}_n(t)$ and $\dot{x}_{n+1}(t)$ into it, one obtains differential equations of forced

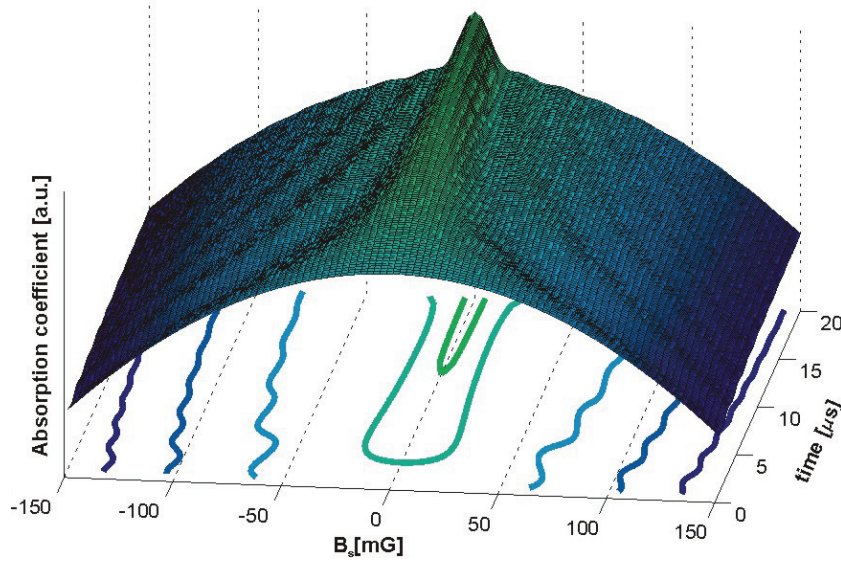


Figure 5. Dependence of the exact solution of EIA, i.e. absorption coefficient, on time and magnetic field B_s . The presented results are for linearly polarized light, $\Gamma = 2\pi 6$ MHz, $\Omega = 0.015\Gamma$ and $\gamma = 0.003\Gamma$. Note that there is a cutoff at the beginning of the time scale.

damped harmonic oscillators in matrix form:

$$\ddot{x}_{n+1}(t) - A_0^2 x_{n+1}(t) = (A_{\text{pert}} A_0 + A_0 A_{\text{pert}}) x_n(t) + A_{\text{pert}}^2 x_{n-1}(t). \quad (7)$$

It is apparent that each correction of each density-matrix element performs forced oscillations, where the damping force (right side) is a linear combination of corrections to density-matrix elements.

Our analysis shows that the evolution of corrections of all density-matrix elements, and therefore the sum of corrections, is of the form

$$\text{sol}_n(t) = \alpha_0 + \sum_i \left(\beta_i + \sum_k \gamma_{i,k} t^k \right) e^{\omega_i t}, \quad (8)$$

where α_0 , β_i , $\gamma_{i,k}$ and ω_i are generally complex numbers, and $k \leq n - 2$. The last sum on the right-hand side of equation (8) appears only for higher-order corrections ($n \geq 3$).

The complex function $e^{\omega t}$ in equation (8), with ω being the complex number $\omega = \omega^R + i\omega^I$, can also be written as

$$e^{\omega t} = \sinh(\omega t) + \cosh(\omega t) = e^{\omega^R t} \cos(\omega^I t) + i e^{\omega^R t} \sin(\omega^I t). \quad (9)$$

The period of $e^{\omega t}$ is given by the imaginary part of ω and is $\frac{2\pi}{\omega^I}$. The real part of ω has to be negative in order for both $e^{\omega^R t}$ to converge to 0 and the solution of correction of the density-matrix element to converge to the steady-state value α_0 (equation (8)). The transient behavior of each density-matrix element is determined by the ratio between the real and imaginary parts of $e^{\omega_i t}$ in equation (8). If the real part is smaller than the imaginary part (absolute values), $e^{\omega t}$ shows oscillations (the oscillator is under-damped), whereas for $|\omega^R| > |\omega^I|$ there are no oscillations

Table 1. Complex frequencies of all density-matrix elements related to harmonic oscillators by equation (7). m and n in the last three rows stand for magnetic quantum numbers. Density-matrix elements are separated into three groups by horizontal lines. The first and second groups are slow-evolving elements ($\propto e^{-\gamma t}$). The second group only gives elements for which the ratio of real and imaginary parts depends on the magnetic field B_s . The third group represents fast-evolving elements, optical coherences, and excited-state populations and coherences ($\propto e^{-\Gamma t}$ or $e^{-\Gamma/2t}$).

Density-matrix element	Complex frequency, ω
$\rho_{g_{-1},g_{-1}}, \rho_{g_0,g_0}, \rho_{g_{+1},g_{+1}}$	$-\gamma$
$\rho_{g_{-1},g_{+1}}$	$-\gamma + i \frac{2l_{F_g} \mu_B}{\hbar} B_s$
$\rho_{g_{+1},g_{-1}}$	$-\gamma - i \frac{2l_{F_g} \mu_B}{\hbar} B_s$
ρ_{g_m, e_n}	$-\gamma - \frac{\Gamma}{2} + i \frac{\mu_B (l_{F_c} n - l_{F_g} m)}{\hbar} B_s$
ρ_{e_m, g_n}	$-\gamma - \frac{\Gamma}{2} + i \frac{\mu_B (l_{F_g} n - l_{F_c} m)}{\hbar} B_s$
ρ_{e_m, e_n}	$-\gamma - \Gamma + i \frac{\mu_B l_{F_c} (n-m)}{\hbar} B_s$

and $e^{\omega t}$ follows exponential decay (the oscillator is over-damped). Note that the contributions from the terms $t^k e^{\omega_i(t)}$ in equation (8) are negligible for the time interval considered here. In the following discussion, we will neglect their influence.

Equation (7) represents a non-homogeneous system of equations. Complex frequencies ω_i of harmonic oscillators, obtained from the homogeneous part of equation (7), are diagonal elements of matrix A_0 . Complex frequencies from the non-homogeneous part of equation (7) are inherited from the solutions of lower-order corrections. Here, we omit the details of how complex frequencies transfer from lower- to higher-order corrections. All frequencies in equation (8) appearing in a particular correction of a particular density-matrix element are obtained in such an iterative way. As the correction order increases, so does the number of terms, i.e. frequencies in equation (8). The analytical expressions of these matrix elements are given in table 1.

The terms in equation (8) have complex frequencies whose values can be grouped into three groups. The terms with spontaneous emission rate Γ in the real part of the complex frequency of ω_i follow exponential decay and rapidly decay to zero for magnetic fields considered here and because Γ is much larger than γ . Following this short time interval, the evolution of EIA is determined by the evolution of ground-level populations and coherences whose complex frequencies are shown in the first three rows of table 1. In figure 5, we show only the time evolution given by those complex frequencies, when the contributions from all other density-matrix elements are practically zero. For complex frequencies belonging to ground-level coherences, the ratio between the real and imaginary parts of the complex frequency depends on the magnetic field B_s . For smaller B_s , corresponding to the range of magnetic fields of the EIA, $\gamma > \frac{2l_{F_g} \mu_B}{\hbar} B_s$ and the oscillations are over-damped. For larger B_s , the values outside the EIA, the oscillator performs an under-damped oscillation. This is clearly seen in the time dependence of $(\rho_{g_{-1},g_{+1}})_{x_2}(t)$, presented in figure 6 for different values of B_s .

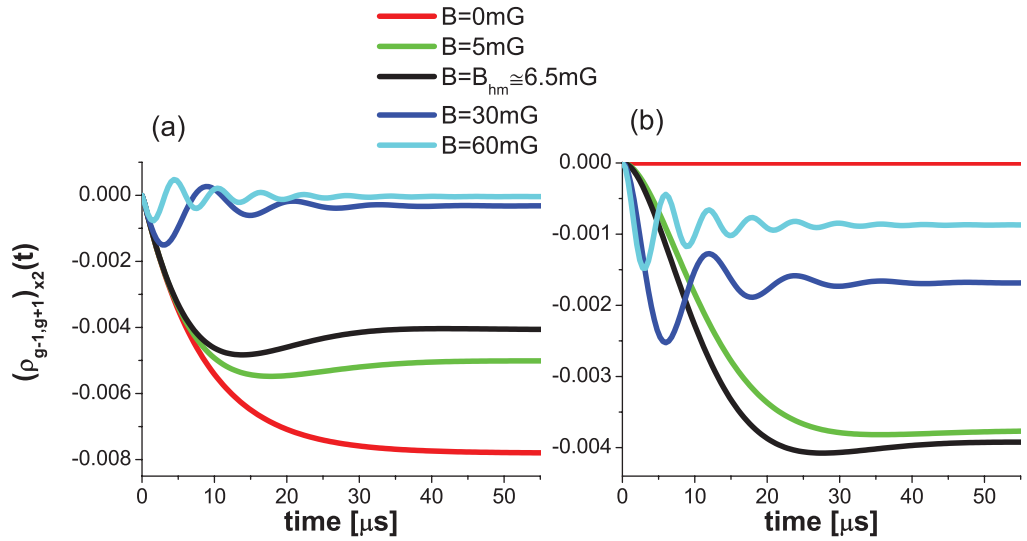


Figure 6. Real (a) and imaginary (b) parts of the time dependence of $(\rho_{g-1,g+1})_{x_2}(t)$ for five magnetic fields. We give dependences for B_s such that two of them are smaller (red and green curves) and two are larger (blue and cyan curves) than B_{hm} (black curve). B_{hm} is the magnetic field corresponding to the half amplitude of the nCL. There are qualitative differences of transient waveforms of $(\rho_{g-1,g+1})_{x_2}$ in these two regions: damped oscillations for $B_s > B_{hm}$ and monotonic decay to a steady-state value for $B_s < B_{hm}$. The presented results are for linearly polarized light, $\Gamma = 2\pi 6$ MHz, $\Omega = 0.015\Gamma$ and $\gamma = 0.003\Gamma$.

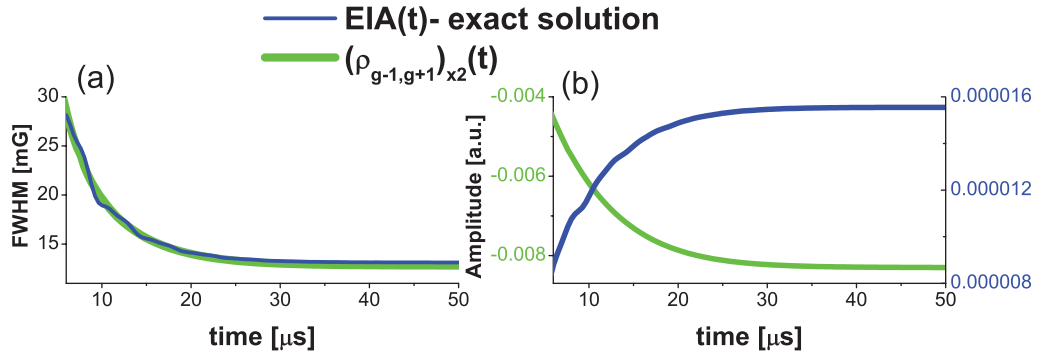


Figure 7. FWHM (a) and amplitude (b) of EIA (blue curves) and the real part of $(\rho_{g-1,g+1})_{x_2}(t)$ (green curves) as a function of time. Note that in (b) there are different scales for amplitudes indicated with different colors (corresponding to blue and green). The presented results are for linearly polarized light, $\Gamma = 2\pi 6$ MHz, $\Omega = 0.015\Gamma$ and $\gamma = 0.003\Gamma$.

In figure 7, we compare the time dependence of $(\rho_{g-1,g+1})_{x_2}(t)$ and of the exact solution for EIA. It can be seen that their amplitudes (with opposite signs) and FWHMs have almost identical time developments. On the other hand, our analysis shows that during the transient

regime, $(\rho_{g_{-1},g_{+1}})_{x_2}(t)$ can be approximated by

$$\begin{aligned} (\rho_{g_{-1},g_{+1}})_{x_2}(t) &\simeq (\rho_{g_{-1},g_{+1}})_{x_2} \left[1 - e^{-(\gamma - i(2l_{F_g}\mu_B/\hbar)B_s)t} \right] \\ &\simeq \text{nCL}(B_s) \left[1 - e^{-(\gamma - i(2l_{F_g}\mu_B/\hbar)B_s)t} \right], \end{aligned} \quad (10)$$

after wide Lorentzians were again replaced with $\frac{1}{\Gamma}$. Due to very similar transient behavior with EIA (figure 7), equation (10) effectively relates the transient behavior of EIA, the time development of its amplitudes and linewidths, with the Lorentzian peak in the steady-state solution of $(\rho_{g_{-1},g_{+1}})_{x_2}(t)$. The analytical expression for transient EIA amplitude can thus be approximated by using equation (10) as $\frac{(\epsilon^2-1)\Omega^2(-2+7b)}{45\Gamma\gamma}(1 - e^{-\gamma t})$. For EIA's FWHM, a transcendental equation is obtained which has no analytical solution.

From the time-dependent analysis of EIA by a perturbative method, we have found that the transient behavior of EIA is influenced by the transient behavior of ground-level Zeeman coherences. We see that a narrow Lorentzian peak, which appears in the steady solutions of $(\rho_{g_{-1},g_{+1}})_{x_2}$ and in EIA, plays a role in their time-dependent behavior. Their time dependence shows over-damped oscillations, as opposed to under-damped oscillations of their pedestals.

4. Conclusion

Steady-state and time-dependent perturbation methods were used to describe the development of EIA. For this study, we used the closed $F_g = 1 \rightarrow F_e = 2$ transition in the Hanle configuration. The analytical expressions of the perturbative method present a strong dependence of EIA on coherences developed in ground-state Zeeman sublevels, and on the efficiency of spontaneous coherence transfer. This method allowed us to follow the transfer of the narrow Lorentzian found in the analytical expression of the second correction of ground-level Zeeman coherences, $(\rho_{g_{-1},g_{+1}})_{x_2}$, as a function of external magnetic field, to higher-order corrections of other density-matrix elements, and to the EIA. The behavior of EIA closely follows the behavior of the peak in $(\rho_{g_{-1},g_{+1}})_{x_2}$. If spontaneous emission of coherences from the excited-state Zeeman sublevels is suppressed, the steady-state resonances of both ground-state Zeeman coherences and optical coherences change sign and the process leads to EIT. Since the atomic scheme $F_g = 1 \rightarrow F_e = 2$ does not have dark states among the ground-state sublevels, EIT, which appears when spontaneous transfer is suppressed, is not due to CPT, but due to the interference between the amplitudes of ground-state Zeeman sublevels.

The time-dependent perturbation method shows similar, over-damped oscillations of the narrow Lorentzian in $(\rho_{g_{-1},g_{+1}})_{x_2}(t)$ and of the EIA, contrary to the under-damped oscillations of the same density-matrix elements, but for magnetic fields outside narrow peaks. The same expression and parameters that define the steady-state linewidths of the second correction of the ground-level Zeeman coherences, and of the EIA, $\frac{\gamma\hbar}{l_{F_g}\mu_B}$, define the critical magnetic field at which the transient behavior of EIA changes from over-damped to damped oscillations.

Acknowledgments

This work was supported by the Ministry of Science and Technological Development of the Republic of Serbia, under grant number III45016. We thank A Kovačević for a careful reading of the manuscript.

Appendix A. Optical Bloch equations

OBEs were solved for linearly polarized light $\vec{E}(\vec{r}_0, t) = \vec{e}_x \cos(\omega t) E_{0x}$ directed along the x -axis and for magnetic field \vec{B} along the z -axis. The quantization axis is along the z -axis. In explicit form, the OBEs stand:

$$\begin{aligned}
\dot{\rho}_{e_i, e_j} &= i(\omega_{e_j} - \omega_{e_i}) \rho_{e_i, e_j} + \frac{iE_{0x}}{2\sqrt{2}\hbar} \sum_{k=-F_g}^{F_g} [\tilde{\rho}_{e_i, g_k} (-\mu_{g_k, e_j, -1} + \mu_{g_k, e_j, +1}) + (\mu_{e_i, g_k, -1} - \mu_{e_i, g_k, +1}) \tilde{\rho}_{g_k, e_j}] \\
&\quad - \Gamma \rho_{e_i, e_j} - \gamma \rho_{e_i, e_j}, \\
\dot{\tilde{\rho}}_{e_i, g_j} &= i(\omega_L + \omega_{g_j} - \omega_{e_i}) \tilde{\rho}_{e_i, g_j} + \frac{iE_{0x}}{2\sqrt{2}\hbar} \\
&\quad \times \left\{ \sum_{k=-F_e}^{F_e} [\rho_{e_i, e_k} (-\mu_{e_k, g_j, -1} + \mu_{e_k, g_j, +1}) + \sum_{k=-F_g}^{F_g} [(\mu_{e_i, g_k, -1} - \mu_{e_i, g_k, +1}) \rho_{g_k, g_j}] \right\} \\
&\quad - \frac{\Gamma}{2} \tilde{\rho}_{e_i, g_j} - \gamma \tilde{\rho}_{e_i, g_j}, \\
\dot{\tilde{\rho}}_{g_j, e_i} &= i(-\omega_L + \omega_{e_i} - \omega_{g_j}) \tilde{\rho}_{g_j, e_i} + \frac{iE_{0x}}{2\sqrt{2}\hbar} \\
&\quad \times \left\{ \sum_{k=-F_g}^{F_g} [\rho_{g_j, g_k} (-\mu_{g_k, e_i, -1} + \mu_{g_k, e_i, +1})] + \sum_{k=-F_e}^{F_e} [(\mu_{g_j, e_k, -1} - \mu_{g_j, e_k, +1}) \rho_{e_k, e_i}] \right\} \\
&\quad - \frac{\Gamma}{2} \tilde{\rho}_{g_j, e_i} - \gamma \tilde{\rho}_{g_j, e_i}, \\
\dot{\rho}_{g_i, g_j} &= i(\omega_{g_j} - \omega_{g_i}) \rho_{g_i, g_j} \\
&\quad + \frac{iE_{0x}}{2\sqrt{2}\hbar} \sum_{k=-F_e}^{F_e} [\tilde{\rho}_{g_i, e_k} (-\mu_{e_k, g_j, -1} + \mu_{e_k, g_j, +1}) + (\mu_{g_i, e_k, -1} - \mu_{g_i, e_k, +1}) \tilde{\rho}_{e_k, g_j}] \\
&\quad - (2F_g + 1) \Gamma \sum_{q=-1}^{q=+1} [b + (1 - b) \delta_{ij}] \mu_{e_{i+q}, g_i, q} \mu_{e_{j+q}, g_j, q}^* \rho_{e_{i+q}, e_{j+q}} \\
&\quad - \gamma \left[\rho_{g_i, g_j} - \frac{1}{(2F_g + 1)} \delta_{ij} \right]. \tag{A.1}
\end{aligned}$$

Appendix B. Derivation of equation (5)

We start from equation (4). A new matrix $P = -A_0^{-1} A_{\text{pert}}$ is introduced that has dimensions 64×64 . Matrix P has elements with indices from (g_{-1}, g_{-1}) to (e_{+2}, e_{+2}) corresponding to density-matrix elements of ρ . Matrix P and all the other presented results are obtained by using the application for analytical calculations.

The solution for zeroth-order correction x_0 is equal populations among the ground states by $1/3$. From equation (4) the second correction is $x_2 = P^2 x_0$, which for $\rho_{g_{-1}, g_{+1}}$ yields the

Table B1. Analytical expressions for elements of matrix P that were used to calculate equation (5).

Element of matrix P	Analytical expression
$\frac{P_{(g-1, e_0), (g-1, g-1)}}{-1-\epsilon}, -\frac{P_{(e_0, g+1), (g+1, g+1)}}{1-\epsilon}$	$-\frac{i\sqrt{\frac{2}{15}}\Omega}{2\gamma+\Gamma-i\frac{2F_g\mu_B}{\hbar}B_s}$
$\frac{P_{(g-1, g+1), (e-1, g_0)}}{-1-\epsilon}, -\frac{P_{(g-1, g+1), (g_0, e+1)}}{1-\epsilon}$	$-\frac{ib\Gamma\Omega}{2\sqrt{10}(\gamma+\Gamma-i\frac{2F_g\mu_B}{\hbar}B_s)(\gamma-i\frac{2F_g\mu_B}{\hbar}B_s)}$
$\frac{P_{(g_0, e+1), (g_0, g_0)}}{-1-\epsilon}, -\frac{P_{(e-1, g_0), (g_0, g_0)}}{1-\epsilon}$	$-\frac{i\sqrt{\frac{7}{5}}\Omega}{2\gamma+\Gamma-i\frac{2F_g\mu_B}{\hbar}B_s}$
$\frac{P_{(g-1, g+1), (e-2, g-1)}}{-1-\epsilon}, -\frac{P_{(g-1, g+1), (g+1, e+2)}}{1-\epsilon}$	$-\frac{ib\Gamma\Omega}{6\sqrt{5}(\gamma+\Gamma-i\frac{2F_g\mu_B}{\hbar}B_s)(\gamma-i\frac{2F_g\mu_B}{\hbar}B_s)}$
$\frac{P_{(g+1, e+2), (g+1, g+1)}}{-1-\epsilon}, -\frac{P_{(e-2, g-1), (g-1, g-1)}}{1-\epsilon}$	$-\frac{2i\Omega}{\sqrt{5}(2\gamma+\Gamma-i\frac{4F_g\mu_B}{\hbar}B_s+i\frac{2F_g\mu_B}{\hbar}B_s)}$
$\frac{P_{(g-1, g+1), (e_0, g+1)}}{-1-\epsilon}, -\frac{P_{(g-1, g+1), (g-1, e_0)}}{1-\epsilon}$	$-\frac{ib\Gamma\Omega}{\sqrt{30}(\gamma+\Gamma-i\frac{2F_g\mu_B}{\hbar}B_s)(\gamma-i\frac{2F_g\mu_B}{\hbar}B_s)}$
	$-\frac{i\Omega}{\sqrt{30}(-\gamma+i\frac{2F_g\mu_B}{\hbar}B_s)}$

following terms,

$$\begin{aligned}
(\rho_{g-1, g+1})_{x_2} = & \frac{1}{3} [P_{(g-1, g+1), (e_0, g+1)} P_{(e_0, g+1), (g+1, g+1)} + P_{(g-1, g+1), (e-1, g_0)} P_{(e-1, g_0), (g_0, g_0)} \\
& + P_{(g-1, g+1), (e-2, g-1)} P_{(e-2, g-1), (g-1, g-1)} + P_{(g-1, g+1), (g_0, e+1)} P_{(g_0, e+1), (g_0, g_0)} \\
& + P_{(g-1, g+1), (g-1, e_0)} P_{(g-1, e_0), (g-1, g-1)} + P_{(g-1, g+1), (g+1, e+2)} P_{(g+1, e+2), (g+1, g+1)}] \quad (\text{B.1})
\end{aligned}$$

or can be expressed through x_1 from $x_2 = P x_1$ as

$$\begin{aligned}
(\rho_{g-1, g+1})_{x_2} = & (\rho_{e_0, g+1})_{x_1} P_{(g-1, g+1), (e_0, g+1)} + (\rho_{e-1, g_0})_{x_1} P_{(g-1, g+1), (e-1, g_0)} + (\rho_{e-2, g-1})_{x_1} P_{(g-1, g+1), (e-2, g-1)} \\
& + (\rho_{g_0, e+1})_{x_1} P_{(g-1, g+1), (g_0, e+1)} + (\rho_{g-1, e_0})_{x_1} P_{(g-1, g+1), (g-1, e_0)} + (\rho_{g+1, e+2})_{x_1} P_{(g-1, g+1), (g+1, e+2)}. \quad (\text{B.2})
\end{aligned}$$

Equation (5) can be obtained from either equation (B.1) or equation (B.2) where analytical expressions for elements of matrix P can be found in table B1.

References

- [1] Alzetta G, Moi L and Orriols G 1979 *Nuovo Cimento B* **52** 209
- [2] Arimondo E 1996 *Prog. Opt.* **35** 257
- [3] Aspect A, Arimondo E, Kaiser R, Vansteenkiste N and Cohen-Tannoudji C 1988 *Phys. Rev. Lett.* **61** 826
- [4] Stephen Harris E 1997 *Phys. Today* **50** 36
- [5] Akulshin A M, Barreiro S and Lezama A 1998 *Phys. Rev. A* **57** 2996
- [6] Lezama A, Barreiro S and Akulshin A M 1999 *Phys. Rev. A* **59** 4732
- [7] Andreeva C, Cartaleva S, Dancheva Y, Biancalana V, Burchianti A, Marinelli C, Mariotti E, Moi L and Nasyrov K 2002 *Phys. Rev. A* **66** 012502
- [8] Kim S K, Moon H S, Kim K and Kim J B 2003 *Phys. Rev. A* **68** 063813

- [9] Chou H-S and Evers J 2010 *Phys. Rev. Lett.* **104** 213602
- [10] Renzoni F, Zimmermann C, Verkerk P and Arimondo E 2001 *J. Opt. B: Quantum Semiclass. Opt.* **3** S7
- [11] Rautian S G 1999 *J. Exp. Theor. Phys.* **88** 6
- [12] Taichenachev A V, Tumaikin A M and Yudin V I 1999 *Phys. Rev. A* **61** 011802R
- [13] Goren C, Wilson-Gordon A D, Rosenbluh M and Friedmann H 2004 *Phys. Rev. A* **69** 053818
- [14] Goren C, Wilson-Gordon A D, Rosenbluh M and Friedmann H 2003 *Phys. Rev. A* **67** 033807
- [15] Zigdon T, Wilson-Gordon A D and Friedmann H 2008 *Phys. Rev. A* **77** 033836
- [16] Dimitrijević J, Arsenović D and Jelenković B M 2007 *Phys. Rev. A* **76** 013836
- [17] Dimitrijević J, Grujić Z, Mijailović M, Arsenović D, Panić B and Jelenković B M 2008 *Opt. Exp.* **16** 1343
- [18] Dimitrijević J, Krmpot A, Mijailović M, Arsenović D, Panić B, Grujić Z and Jelenković B M 2008 *Phys. Rev. A* **77** 013814
- [19] Renzoni F, Lindner A and Arimondo E 1999 *Phys. Rev. A* **60** 450
- [20] Chen H X, Durrant A V, Marangos J P and Vaccaro J A 1998 *Phys. Rev. A* **58** 1545
- [21] Li Y-Q and Xiao M 1995 *Opt. Lett.* **20** 1489
- [22] Valente P, Failache H and Lezama A 2002 *Phys. Rev. A* **65** 023814
- [23] Valente P, Failache H and Lezama A 2003 *Phys. Rev. A* **67** 013806
- [24] Scully M O and Zubairy M S 1997 *Quantum Optics* (Cambridge: Cambridge University Press)
- [25] Decomps B, Dumont M and Ducloy M 1976 *Linear and Nonlinear Phenomena in Laser Optical Pumping (Laser Spectroscopy of Atoms and Molecules vol 2)* ed H Walther (Berlin: Springer) p 283
- [26] Cohen-Tannoudji C, Dupont-Roc J and Grynberg G 1992 *Atom-Photon Interactions: Basic Processes and Applications* (New York: Wiley-Interscience)
- [27] Korsunsky E A and Kosachiov D V 1999 *Phys. Rev. A* **60** 4996
- [28] Taichenachev A V, Tumaikin A M, Yudin V I and Nienhuis G 2004 *Phys. Rev. A* **69** 033410
- [29] Goren C, Wilson-Gordon A D, Rosenbluh M and Friedmann H 2004 *Phys. Rev. A* **70** 043814